applied sciences

MDPI

Article

Advancement of Finite Element Method Solver Used in Dam Safety Monitoring System by Interpolation of Pore Pressure and Temperature Values

Snezana Vulovic [1], Marko Topalovic [1,*], Miroslav Zivkovic [2], Dejan Divac [3] and Vladimir Milivojevic [3]

[1] Institute of Information Technologies, University of Kragujevac, 34000 Kragujevac, Serbia; vsneza@kg.ac.rs
[2] Faculty of Engineering, University of Kragujevac, 34000 Kragujevac, Serbia; miroslav.zivkovic@kg.ac.rs
[3] Jaroslav Černi Water Institute, 11000 Belgrade, Serbia; dejan.divac@jcerni.rs (D.D.); vladimir.milivojevic@jcerni.rs (V.M.)
* Correspondence: topalovic@kg.ac.rs

Featured Application: Featured Application: The algorithms and procedures presented in this paper were developed to increase robustness of FEM solvers used in Dam Monitoring Systems, allowing easy adaptation by inclusion of new measuring points.

Abstract: In this paper, we focused on the advancement of Dam Monitoring Software that incorporates the Finite Element Method (FEM), as these large infrastructure constructions are crucial for ensuring a dependable water supply, irrigation, flood control, renewable electric energy generation, and safe operation, which is of utmost importance to any country. However, the material properties and geotechnical environments of dams can change (deteriorate) over time, while the standards and legal norms that govern them become more and more rigorous, so in order to accurately assess the state of a dam and detect any concerning behavior, the software must be updated as well. The custom-developed FEM solver, unlike many commercial alternatives, is adaptable and can be reconfigured to function within a Dam Monitoring System. In this paper, we present the procedure for interpolating numerical values at measurement points, when the position of the measurement point does not align with the node of the element, allowing for additional instrument locations to be added to the monitored system without the need for remeshing the numerical model. This procedure is used to compare the actual pore pressures and temperature values of the concrete dam structure with the prediction of the numerical model, and the agreement is much greater with the new interpolation algorithm in comparison to the nearest nodal values, with the average relative difference for pore pressure reduced from 8.89% to 8.10%, justifying this implementation.

Keywords: finite element method; finite element interpolation; piezometer measurements; dam monitoring system; structural health monitoring; hydrological monitoring

Citation: Vulovic, S.; Topalovic, M.; Zivkovic, M.; Divac, D.; Milivojevic, V. Advancement of Finite Element Method Solver Used in Dam Safety Monitoring System by Interpolation of Pore Pressure and Temperature Values. *Appl. Sci.* **2024**, *14*, 9680. https://doi.org/10.3390/app14219680

Academic Editors: Francesco Duronio and Angelo De Vita

Received: 31 August 2024
Revised: 14 October 2024
Accepted: 17 October 2024
Published: 23 October 2024

1. Introduction

The construction of a dam and the formation of a reservoir upstream can provide multiple benefits, including the use of the dammed watercourse for processing into drinking water [1], irrigation [2], electricity generation [3], and flood control [3]. Ensuring the safety of a dam is crucial for the protection of private and public property, the environment, and the economic development of the surrounding area [2]. Safety regulations for dams [4] aim to ensure that they can perform their intended functions without causing harm to people, the environment, or property [5]. Like all structures, dams have a limited lifespan [6] and can be affected by changes in operating conditions (due to climate change) [7], construction materials [8], and the geotechnical environment over time [9]. In addition, social and

professional factors that impact safety criteria and risk may change, often as a result of changes in standards and legal norms. The need to monitor the condition of a dam over time [10] becomes more important as the material ages and deteriorates [8], especially in light of the increasing frequency of extreme droughts and floods due to climate change [11]. These floods and droughts can significantly increase or decrease ground water levels, and consequently values of pore pressure. Dams that were built decades ago now face more extreme load cases, which were far more favorable at the time of their construction.

The technical monitoring of a dam using measuring instruments [12] is a crucial part of dam operation management, with the goal of preventing the possibility of damage, collapse, and uncontrolled water discharge [13]. The purpose of technical observation is to measure a range of relevant values and determine whether the actual condition of the dam is consistent with the predicted behavior [10]. Hence, the goal of data collection is to provide sufficient information to identify and detect processes that could compromise the safety of the facility [14]. The system for technical monitoring and data collection has evolved over time [15], leading to the need for standardization of data [14]. As a result, the collection, acquisition, archiving, processing, and use of technical monitoring data form a modern Dam Monitoring System (DMS) [16]. The concept of dam safety management includes a series of procedures designed to create a physically based, software-supported system that will ensure the collection of all data that are important for dam safety [16]. The analysis and interpretation of these data through mathematical models of relevant processes allow for the identification of appropriate actions to ensure the safety and stability of dams.

Mathematical models for predicting the behavior of dams [17] are an important part of DMSs and their improvement is the main focus of this paper. These models provide an estimated response of a dam to a given load and can be compared with measurements to determine the safety of the dam [18]. There are several types of models that can be used to predict dam behavior, including statistical models [19], deterministic models, and mixed hybrid mathematical models [20]. Statistical models are based solely on past monitoring data and explain the relationship between loads and dam behavior [21]; however, their parameters do not have physical meaning [22]. Models based on multiple linear regression (MLR) are commonly used for prediction due to their simplicity and quick calculation [23]. Deterministic models, on the other hand, require the solution of differential equations. Solving closed-form differential equations can be difficult, so many models are based on numerical methods such is the Finite Element Method (FEM) [24–28].

An example of FEM-based software used in geomechanics, GeoStudio Core, includes specialized solvers: SLOPE/W [29], SEEP/W [30], and SIGMA/W [31].

PLAXIS is another well-known advanced three-dimensional geotechnical engineering software that uses finite element analysis [32,33].

General purpose FEM solvers like ABAQUS and Ansys can also be used in geo-engineering [34–37].

A disadvantage of previously described commercial general purpose and specialized FEM software is its difficult integration into DMSs.

Custom-made FEM solvers, such as 3DFE, have been developed for automatic monitoring data analysis and dynamic analysis of dam–reservoir–foundation systems, using a solid–fluid coupled formulation to account for dam–water interactions, and include modules for complex modal and seismic analysis [38].

In commercial software such as Ansys or ABAQUS, meshing/remeshing is performed in just a few mouse clicks, but, unfortunately, academic, research-oriented, open source, and highly specialized FEM software lack such capabilities. The algorithm presented in this paper can easily be added to any FEM software, increasing simulation accuracy, while removing the need for intricate remeshing.

This paper presents a novel and original implementation of an interpolation algorithm used as a solution to the problem of subsequent modification of existing FEM dam models in DMSs. Its relevance and contribution lie in the possibility of improving countless FEM

codes with a simple algorithm which fills the narrow gap between commercial FEM solvers and academic, research-oriented, open source, and highly specialized commercial software, such as that used for DMS.

This algorithm can be used in the analysis of other FEM problems as well, not just for geomechanics, but it is applicable for FEM only; other numerical methods such as FVM or SPH use similar yet different discretization of continua, which means the interpolation showcased in this paper cannot be implemented.

The remainder of this paper is structured as follows:

Section 2, "Materials and Methods", describes the Hydropower Plant Djerdap and the finite element model used for its DMS. Section 3, "Natural coordinate of the point in tetrahedral element", showcases the interpolation functions for the tetrahedral finite element and presents the algorithm for determining the local coordinates of a particular point within that element. Section 4, "Calculation of potential at measurement points position", outlines the procedure for calculating the potential at measurement points. In Section 5, "Results and Discussion", the results of pore pressure calculation and temperature analysis are presented, and improvements over the old methodology using approximated values calculated at nodes are discussed. Finally, Section 6, "Conclusions", summarizes the motivation behind this work, improvements to non-commercial software, and implications for DMS accuracy.

2. Materials and Methods

The new algorithm will be showcased on the DMS for the Hydropower Plant Djerdap (HPP Djerdap), which is a medium-head concrete dam located on the Danube River approximately 943 km upstream from the river's estuary into the Black Sea. The dam is 1278 m long, 55 m high, and has a base width of 46 m. It was constructed jointly by Romania and the former Yugoslavia in 1970 and is now operated by Serbia and Romania, each with six generators, seven spillways, and a ship lift. The power output of the Hydropower Plant Djerdap depends on the amount of rainfall in the Danube River basin, with an average annual production of 6000 GWh, which accounts for approximately 20% of Serbia's electricity generation [39,40].

To model the thermal, filtration, and stress-deformation processes at the Hydropower Plant Djerdap dam (Figure 1), a three-dimensional finite element model of the dam was created (Figures 2 and 3). The model was based on the dam's three-dimensional geometric model, the engineering–geological structure of the surrounding terrain, and the exploitation conditions of the terrain, which was divided into eight geological areas. The dimensions of the model are 400 × 442 × 50 m. Upstream and downstream ranges are both 200 m. The FEM model includes the spillway (on the right in Figures 1 and 2) and power plant (on the left in Figures 1 and 2). To accurately capture the dam's behavior with as few elements as possible, the model used a very fine mesh for the dam and a coarser mesh for the surrounding terrain, with the mesh becoming increasingly coarse further from the dam. The finite element mesh of the model was created using tetrahedral finite elements with intermediate nodes (10 nodes per element). The structure was modeled in detail with 2,164,778 elements and 3,198,873 nodes. The finite element model of the dam was designed to be integrated into a software system for safety analysis.

Figure 1. The HPP Djerdap.

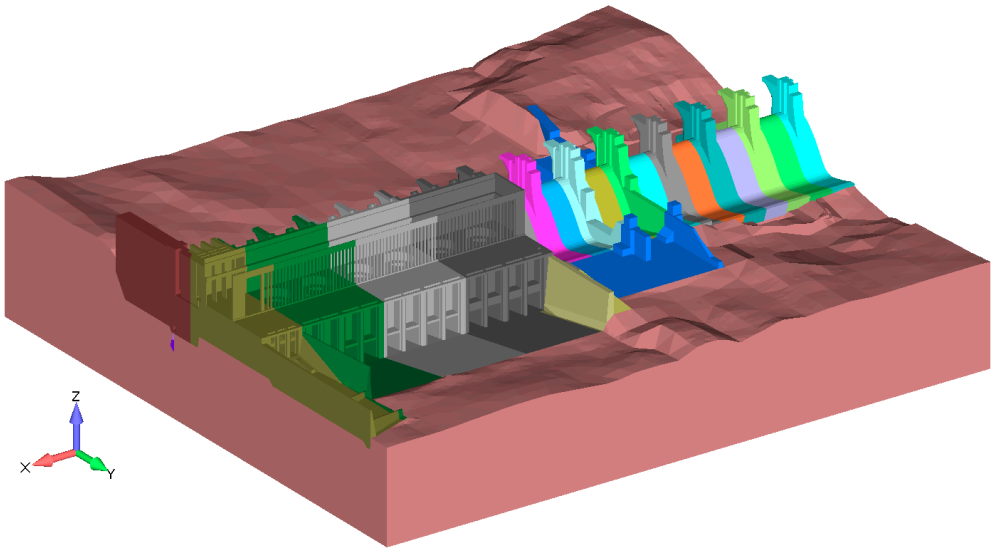

Figure 2. The FEM model of the overflow dam and power plant of HPP Djerdap.

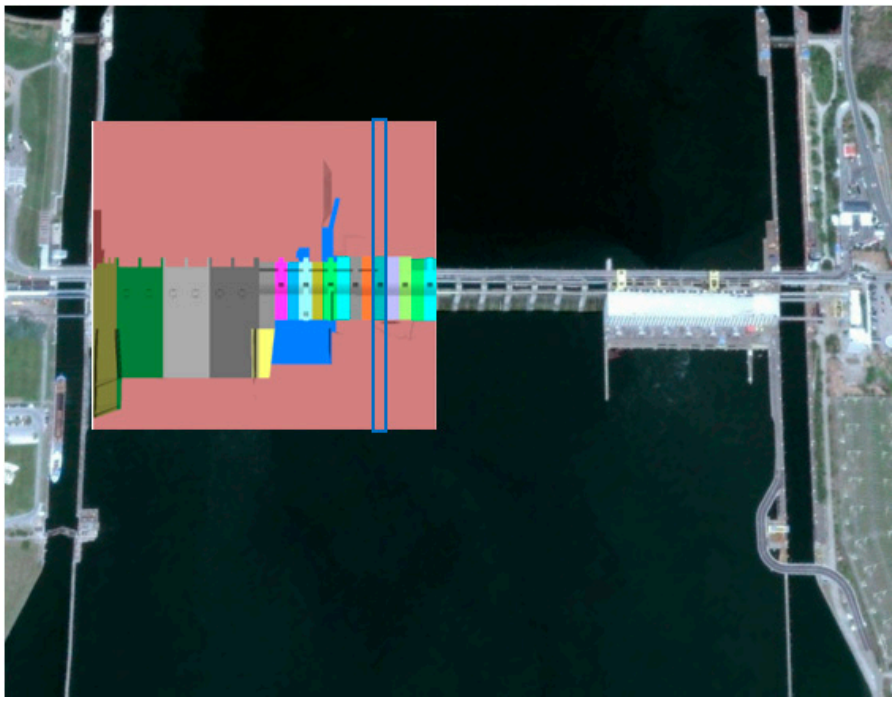

Figure 3. The position of the FEM model of the overflow dam and power plant of HPP Djerdap.

The same finite element model was used for thermal analysis, fluid flow analysis through a porous medium, and stress–strain analysis. The spillway of the dam is divided into sections, known as lamellas. Lamela 10 is marked with the blue box in Figure 3; and will be used to showcase interpolation procedure presented in this paper. In order to include the positions of measuring devices in the FE model for all analyses, it is necessary to include the positions of the thermometers and piezometers. However, incorporating the positions of the measuring points in the FE model (by matching the position of the measuring point with a FE node) can significantly increase the number of elements and nodes in the model. Additionally, the positions of all measuring points may not be known at the time the FE model is created, or new measuring points may need to be added subsequently. Therefore, a procedure for calculating the numerical value (such as temperature, potential, displacement, etc.) when the position of the measuring point does not align with a node in the model was developed. The positions of the thermometers, manometers, and piezometers on lamella ten in the model are shown in Figure 4. Thermometers (labeled as T-x) are marked in Figure 4a, while manometers (labeled as M-x) and piezometers (labeled as P-x), which are both instruments used to measure pressure (P), are marked in Figure 4b. Lamella ten is marked in Figure 3.

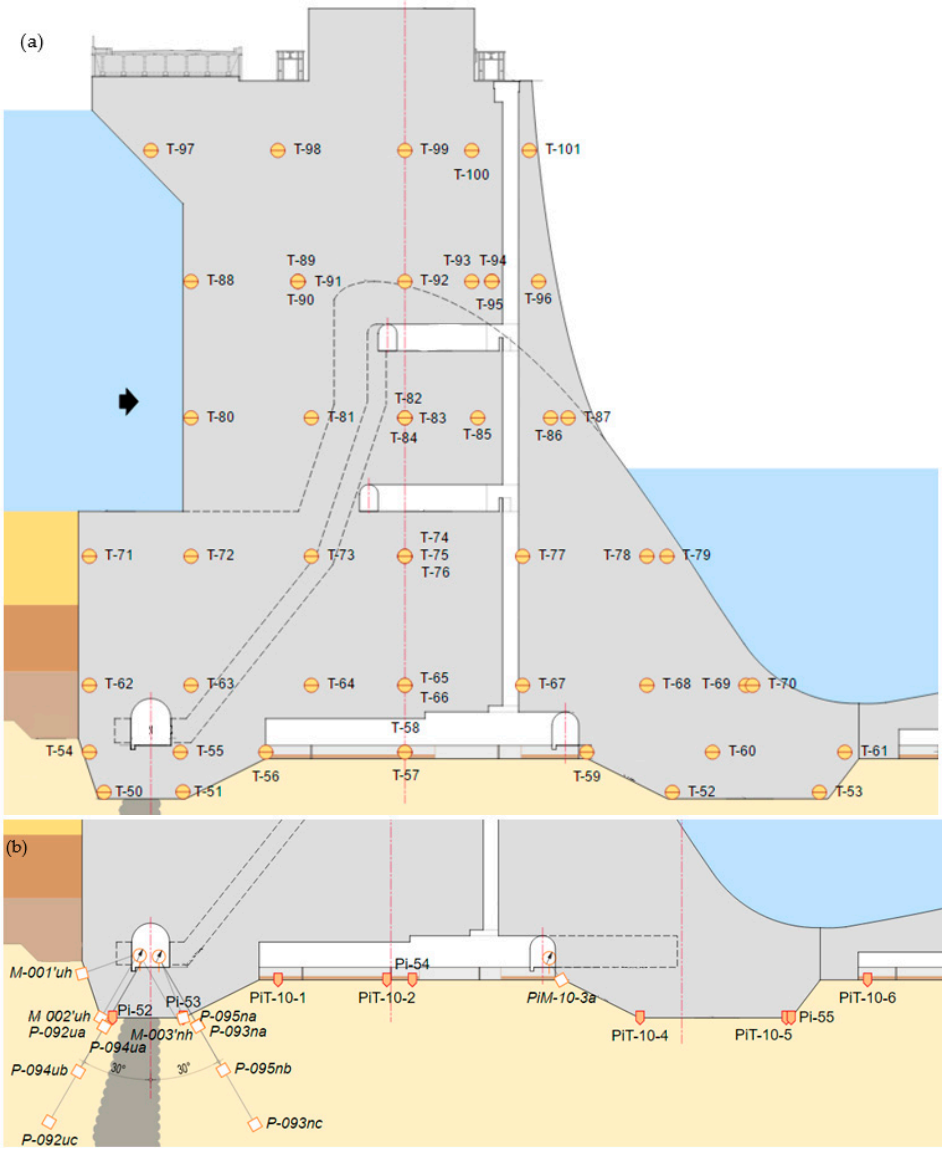

Figure 4. Measuring devices on lamella ten of HPP Djerdap: thermometers (**a**), manometers and piezometers (**b**).

3. Natural Coordinate of Point in Tetrahedral Element

A three-dimensional (3D) hexahedral finite element is commonly used for modeling three-dimensional bodies of general shape. A 3D hexahedral finite element can have a different number of nodes, typically ranging from 8 to 21. For modeling complex, irregular shapes like dams, tetrahedral finite elements with intermediate nodes are often used (Figure 5) [41]. An arbitrary position of a measuring point (M_P) in a tetrahedral element with intermediate nodes is shown in Figure 5.

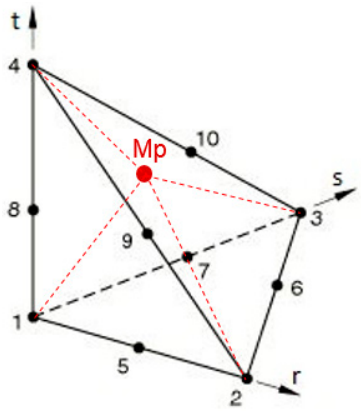

Figure 5. Tetrahedral element with 10 nodes and arbitrary position of measuring point.

Geometry interpolation functions [42] have the following form:

$$\mathbf{x} = \begin{Bmatrix} \mathrm{x} \\ \mathrm{y} \\ \mathrm{z} \end{Bmatrix} = \mathbf{HX} \tag{1}$$

where the variables are defined as follows:

x—is the coordinate vector of the point in the element,

H—is the interpolation matrix,

X—represents vector of node coordinates.

The vector of the node coordinates is given by Equation (2):

$$\mathbf{X}^T = [\mathrm{X}_1\ \mathrm{Y}_1\ \mathrm{Z}_1\ \mathrm{X}_2\ \mathrm{Y}_2\ \mathrm{Z}_2 \ldots\ldots \mathrm{X}_N\ \mathrm{Y}_N\ \mathrm{Z}_N] \tag{2}$$

The interpolation matrix is as follows:

$$\mathbf{H} = \begin{bmatrix} \mathrm{h}_1 & 0 & 0 & \mathrm{h}_2 & 0 & 0 & \ldots\ldots & \mathrm{h}_N & 0 & 0 \\ 0 & \mathrm{h}_1 & 0 & 0 & \mathrm{h}_2 & 0 & \ldots\ldots & 0 & \mathrm{h}_N & 0 \\ 0 & 0 & \mathrm{h}_1 & 0 & 0 & \mathrm{h}_2 & \ldots\ldots & 0 & 0 & \mathrm{h}_N \end{bmatrix} \tag{3}$$

The interpolation functions for the tetrahedral finite element are given in Table 1 [42].

Midnodes of the tetra element are not used to calculate the local coordinates of the measuring point. The coordinates of the measuring point M_P (x, y, z) can be expressed using the coordinates of the element in which it is located, according to Equation (1), as follows:

$$\begin{aligned} x &= (1 - r - s - t)X_1 + rX_2 + sX_3 + tX_4 \\ y &= (1 - r - s - t)Y_1 + rY_2 + sY_3 + tY_4 \\ z &= (1 - r - s - t)Z_1 + rZ_2 + sZ_3 + tZ_4 \end{aligned} \tag{4}$$

with the following definitions:

$X_1, Y_1, Z_1;\ X_2, Y_2, Z_2;\ X_3, Y_3, Z_3;\ X_4, Y_4, Z_4$—the coordinates of the nodes of the tetrahedral element; r, s, t—the local coordinates of the measuring point M_P.

Table 1. Interpolation functions for the tetrahedral finite element.

		i = 5	i = 6	i = 7	i = 8	i = 9	i = 10
h_1	$1-r-s-t$	$-\frac{h_5}{2}$		$-\frac{h_7}{2}$	$-\frac{h_8}{2}$		
h_2	r	$-\frac{h_5}{2}$	$-\frac{h_6}{2}$			$-\frac{h_9}{2}$	
h_3	s		$-\frac{h_6}{2}$	$-\frac{h_7}{2}$			$-\frac{h_{10}}{2}$
h_4	t				$-\frac{h_8}{2}$	$-\frac{h_9}{2}$	$-\frac{h_{10}}{2}$
h_5	$4r(1-r-s-t)$						
h_6	$4rs$						
h_7	$4s(1-r-s-t)$						
h_8	$4t(1-r-s-t)$						
h_9	$4rt$						
h_{10}	$4st$						

By solving the system of Equations (4), natural coordinates are obtained:

$$r = \frac{\left\{ \begin{array}{l} x[Z_1(Y_3-Y_4)+Z_3(Y_4-Y_1)+Z_4(Y_1-Y_3)]+X_1[Y_3(Z_4-z)+y(Z_3-Z_4)+Y_4(z-Z_3)]+ \\ X_3[Y_4(Z_1-z)+y(Z_4-Z_1)+Y_1(z-Z_4)]+X_4[Y_3(z-Z_1)+y(Z_1-Z_3)+Y_1(Z_3-z)] \end{array} \right\}}{\left\{ \begin{array}{l} X_2[Z_1(Y_3-Y_4)+Z_3(Y_4-Y_1)+Z_4(Y_1-Y_3)]+X_1[Y_3(Z_4-Z_2)+Y_2(Z_3-Z_4)+Y_4(Z_2-Z_3)]+ \\ X_3[Y_4(Z_1-Z_2)+Y_1(Z_2-Z_4)+Y_2(Z_4-Z_1)]+X_4[Y_3(Z_2-Z_1)+Y_2(Z_1-Z_3)+Y_1(Z_3-Z_2)] \end{array} \right\}} \quad (5)$$

$$s = \frac{\left\{ \begin{array}{l} x[Z_1(Y_4-Y_2)+Z_2(Y_1-Y_4)+Z_4(Y_2-Y_1)]+X_1[Y_2(z-Z_4)+y(Z_4-Z_2)+Y_4(Z_2-z)]+ \\ X_2[Y_4(z-Z_1)+y(Z_1-Z_4)+Y_1(Z_4-z)]+X_4[Y_2(Z_1-z)+y(Z_2-Z_1)+Y_1(z-Z_2)] \end{array} \right\}}{\left\{ \begin{array}{l} X_2[Z_1(Y_3-Y_4)+Z_3(Y_4-Y_1)+Z_4(Y_1-Y_3)]+X_1[Y_3(Z_4-Z_2)+Y_2(Z_3-Z_4)+Y_4(Z_2-Z_3)]+ \\ X_3[Y_4(Z_1-Z_2)+Y_1(Z_2-Z_4)+Y_2(Z_4-Z_1)]+X_4[Y_3(Z_2-Z_1)+Y_2(Z_1-Z_3)+Y_1(Z_3-Z_2)] \end{array} \right\}} \quad (6)$$

$$t = \frac{-\left\{ \begin{array}{l} [X_3(Y_1-Y_2)+X_1(Y_2-Y_3)+X_2(Y_3-Y_1)][X_2(Z_1-z)+X_1(z-Z_2)+x(Z_2-Z_1)]- \\ [X_2(Y_1-y)+X_1(y-Y_2)+x(Y_2-Y_1)][X_3(Z_1-Z_2)+X_1(Z_2-Z_3)+X_2(Z_3-Z_1)] \end{array} \right\}}{\left\{ \begin{array}{l} -[X_4(Y_1-Y_2)+X_1(Y_2-Y_4)+X_2(Y_4-Y_1)][X_3(Z_1-Z_2)+X_1(Z_2-Z_3)+X_2(Z_3-Z_1)] \\ +[X_3(Y_1-Y_2)+X_1(Y_2-Y_3)+X_2(Y_3-Y_1)][X_4(Z_1-Z_2)+X_1(Z_2-Z_4)+X_2(Z_4-Z_1)] \end{array} \right\}} \quad (7)$$

The FE model of the dam was created using the program Femap [43]. To determine the specific element in the entire model in which a measuring point is located, and to determine the local coordinates of that measuring point, an Application Programming Interface (API) [44] for the Femap program was developed. An API represents a user interface for some implemented functionality that programmers can use to perform various operations [44]. The Femap API is an object-oriented system, meaning that all of the finite element model data are represented as discrete instances of objects that can be interacted with by the user or other software [44]. For each application written, it is necessary to define and reference a Femap application object that controls the connection between the application and the Femap software [43]. The application object includes data and functionality of a global nature, with properties that include all global settings of the Femap session. Almost all functions provided by the Femap software menus are available as methods within the application object [45–47].

The algorithm for determining local coordinates is shown in Figure 6. Before starting the API, a file containing the positions of the measuring points must be loaded into the model. The loaded coordinates of the measuring points are used to generate points in the FE model. When the developed API subroutine is started, the user must first select measurement points and elements in the model. The user can select all elements of the FE model, which would be very inefficient, or a portion of the elements in which the measured points are likely located.

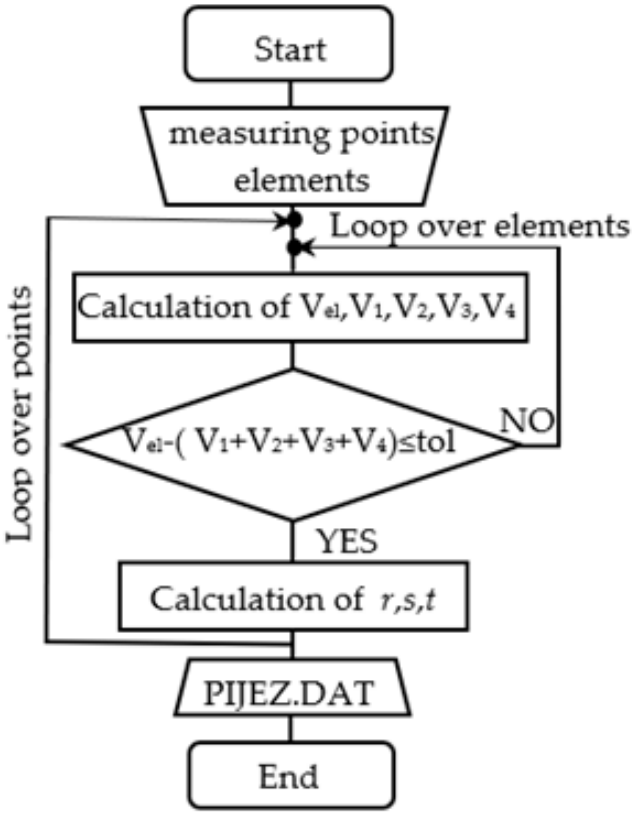

Figure 6. Algorithm for calculation of local coordinates.

In the API subroutine, the first step is to determine the specific element in the model in which the measurement point is located. To do this, "virtual" elements are created from the nodes of the observed element and the measuring point. Practically, a real tetrahedral element is divided into four "virtual" elements with the measuring point as a common node. These "virtual" elements are as follows: 1, 2, 3, M_P; 1, 3, 4, M_P; 1, 2, 4, M_P; and 2, 3, 4, M_P. The volumes of the real element and the "virtual" elements are calculated. If the measurement point is located in an element, the sum of the volumes of the "virtual" elements ($V_1 + V_2 + V_3 + V_4$) will be equal to the volume of the real element (V_{el}), with a tolerance of 0.001 used in the algorithm (Figure 6).

The API creates a new group in the Femap model with measurement points and the corresponding elements. Figure 7 shows the model with marked elements that contain measuring points that monitor the groundwater level. The API also creates an ASCII file called PIJEZ.DAT that includes the designation of the measuring point, the ID of the element, the global coordinates (x, y, z) of the measuring point, and the local coordinates (r, s, t) of the measuring point within the element. A portion of the PIJEZ.DAT file is shown in Figure 8. The location of measuring points designated in Figure 8 can be seen in Figure 4b. Since the locations of the measuring points for temperature, groundwater level, and displacements are not the same, it is necessary to start the API subroutine for determining local coordinates and creating the PIJEZ.DAT file for each group of measuring devices.

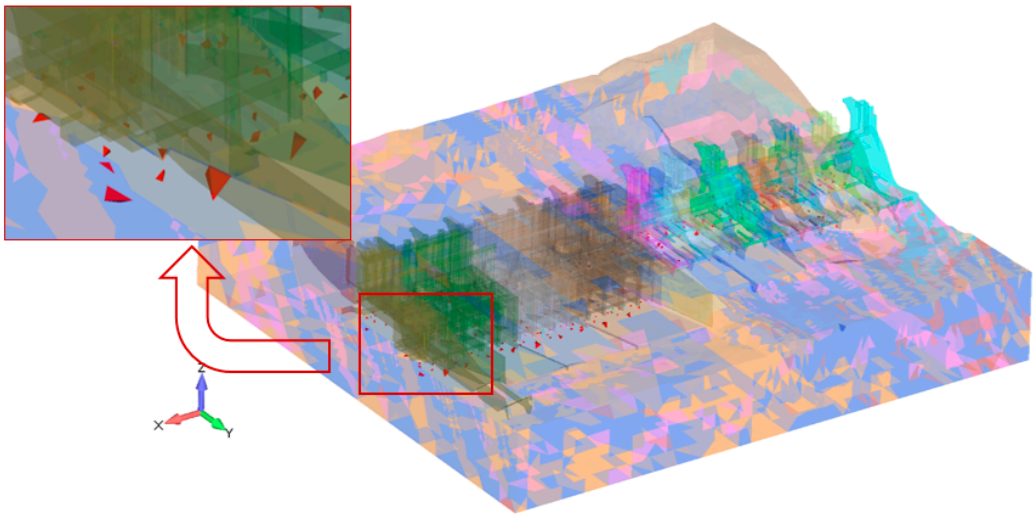

Figure 7. FEM model of dam with highlighted elements of measured points.

Mp	ID el	x	y	y	r	s	t
M-001uh	618969	115.61	-19.92	24.00	0.3	0.28	0.28
M-002uh	625779	115.79	-16.92	19.00	0.2	0.18	0.38
M-003nh	1173745	116.37	-10.42	18.80	0.1	0.68	0.18

Figure 8. Part of PIJEZ.DAT file.

4. Calculation of Potential at Measurement Points Position

For stress–strain analysis, thermal analysis, and now analysis of flow through a porous medium, we used PAK (Program za Analizu Konstrukcija, engl. Software for Structure Analysis), a Multiphysics FEM software developed at the engineering software laboratory at the Faculty of Engineering, University of Kragujevac, Serbia. The implementation of in-house developed software allowed us full access to source code and to improve the program with the algorithms and equations presented in this paper. The PAKS module [48] of PAK-Multiphysics was used for stress–strain analysis, while PAKT was used for thermal analysis [49], and the recently developed module PAKV was used for the analysis of groundwater flow through porous media. These programs were modified to calculate and print numerical values at the measuring points (Figure 9). The input file, pakp.dat, for the PAKV program contains all of the finite element data about the model (nodes, elements, material characteristics, boundary conditions, etc.) and an identifier indicating whether or not to read the measurement points, the locations of which were saved in the file PIJEZ.DAT.

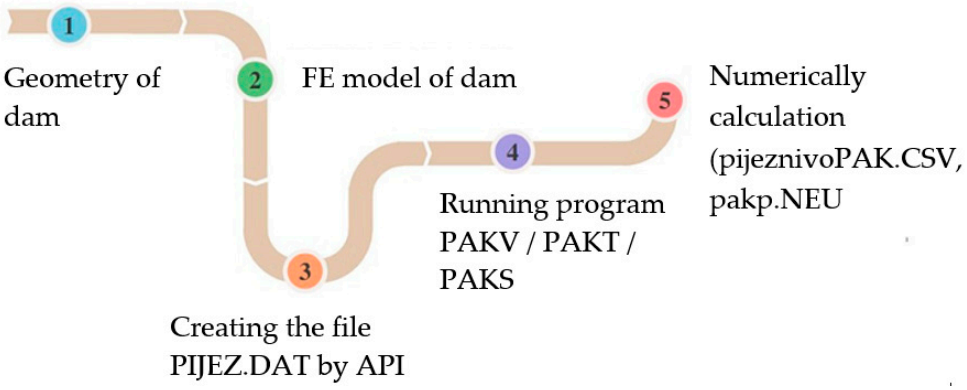

Figure 9. A flow chart of the PAKV/PAKT/PAKS programs.

The potential/temperature at the location of the measuring point is calculated in the print subroutine and written to the file pijeznivoPAK.CSV. The potential/temperature at the measuring point (φ_{M_P}) is calculated by interpolation based on the potential/temperature in the nodes of the element in which it is located and the local coordinates of the measuring point according to Equation (8):

$$\varphi_{M_P} = \sum_{i=1}^{10} h_i \varphi_i \quad (8)$$

The variable definitions are as follows:

h_i—is the interpolation functions given in Table 1,

φ_i—is the potential/temperature in the node i.

The potential values at the measuring points are printed in the file pijeznivoPAK.csv, which contains the designation of the measuring point and the potential.

Points 4 and 5 in the flow chart in Figure 9 are part of the calibration phase. The calibration procedure was performed using a hybrid procedure of the FE model and existing neural networks described in [50,51], as depicted in Figure 10.

The calibration of the FE model was carried out through multi-criteria optimization to minimize the deviation between calculated and observed values for the selected set of parameters. The genetic NSGA-II algorithm was used for multi-criteria optimization.

The input data for neural network training consisted of a limited set of possible combinations of FE model parameters. It was necessary to test the trained neural network with combinations of model parameters that were not used during training. Therefore, additional FE calculations should be performed by randomly selecting parameters. New combinations are generated, and the results of the FE calculations are compared with those given by the neural network. If the results align with the desired accuracy, the trained neural network is used to calibrate the model parameters. Otherwise, the network is re-trained using different parameter ranges or with a different number of hidden neurons.

Once trained, the neural network is used for calibrating model parameters instead of the FE model. For known observed quantities (temperature, potential, etc.), populations are created with individuals that contain the values of the parameters to be calibrated. The evaluation of individuals is performed by calculations on the neural network, rather than the FE model. The goal is to minimize the difference between the calculated and observed values defined through the calibration criterion. When the convergence criterion is met, the best individual contains the calibrated values of the FEM model parameters.

Stationary analysis was used to calibrate the filtration coefficients (PAKV). A bash–python script called wrapper [52] for calibration phase was developed, shown in Figure 11. The input variables in the wrapper are the corrected filtration coefficients (ENTER.CSV, Figure 11), the reservoir water level, and the lower water level (BOUNDARYCON.CSV, Figure 11). Different values of the water level in the reservoir (WLR) and the tailwater (TW) were used for calibration and subsequent verification. Each water level in the reservoir/tailwater corresponds to a prescribed potential on the wetted area of concrete and rock. For the purposes of calibration (and DMS), an algorithm for automatic conditional prescription of boundary conditions was developed. Only one input file is created. The "possible" potential is set at all nodes (NPZAD) of concrete and rock below the elevation of the Full Reservoir Level (FLR) upstream, and the maximum possible elevation of the tailwater downstream. These values are saved in K9-12.DAT file; see Figure 11. During the execution of the PAKV program, a check is performed if the z coordinate of the nodes on which the "possible" potential is prescribed is lower than the set water level in the reservoir and tailwater, i.e., whether the node is wetted. If the node is wetted, the potential is set to be equal to the water level in the reservoir or the tailwater, else it is not prescribed; see Figure 12a. The calculation of the groundwater flow was performed in stationary, which means that in practice, if commercial software was used, it would be necessary to create a new input file with every change in the water level.

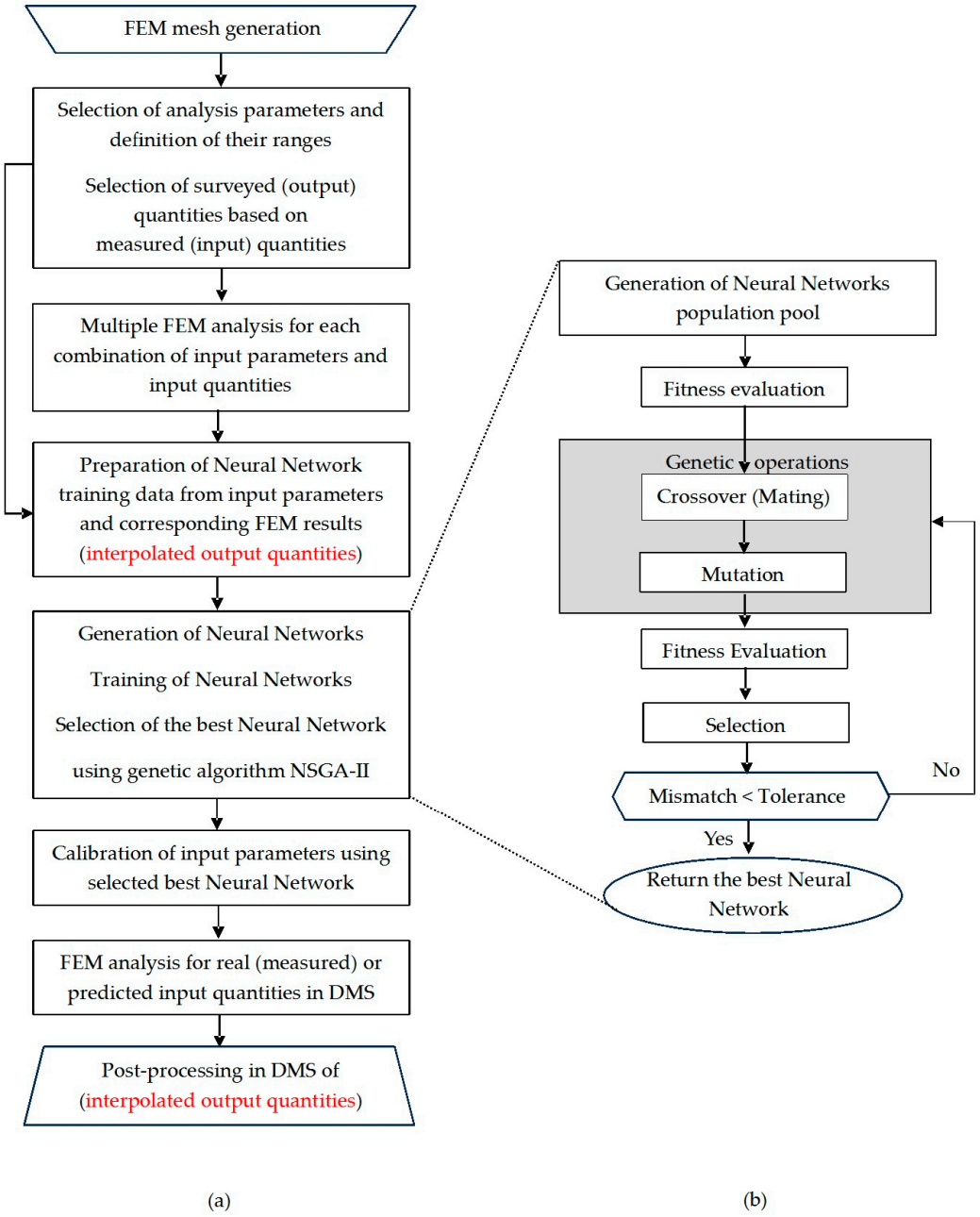

Figure 10. DMS flow chart: (**a**) interpolation algorithm function within DMS, (**b**) genetic algorithm used for neural network training.

During the calibration phase of the FE model, the correction of the FE model's filtration coefficients (ENTER.CSV) was performed based on the difference between the measured and calculated potential values, with the aim of achieving the best match between the measured and numerically obtained values.

Non-stationary analysis was performed to calibrate the values of thermal processes. Boundary conditions were defined for each discrete time step based on historical measurements, which included the following: upper and lower water levels; air temperature at two measuring points; upper water temperature at two measuring points; and foundation temperatures at a larger number of measuring points. On the body of the dam, the conduction concrete–air for the parts above the water was set, while for the submerged parts, the conduction concrete–water was set. The calibration procedure was carried out after the previously completed analysis of the available data.

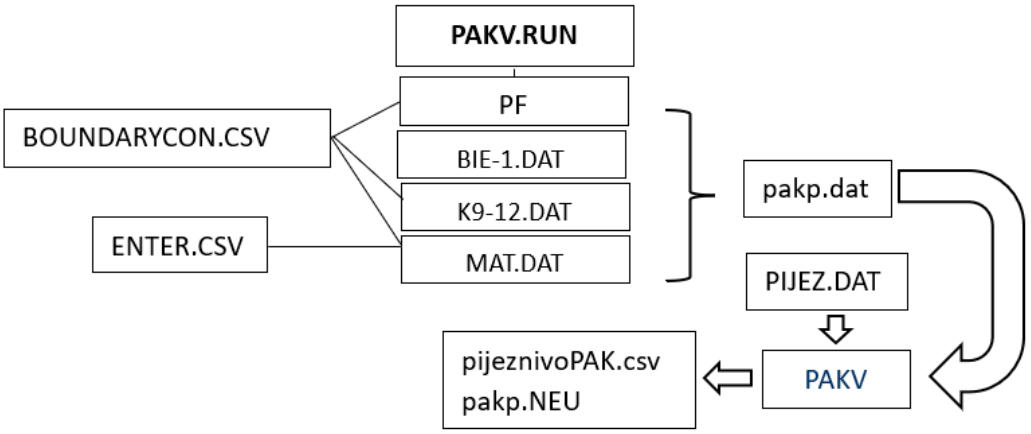

Figure 11. Flow chart of wrapper of PAKV. code.

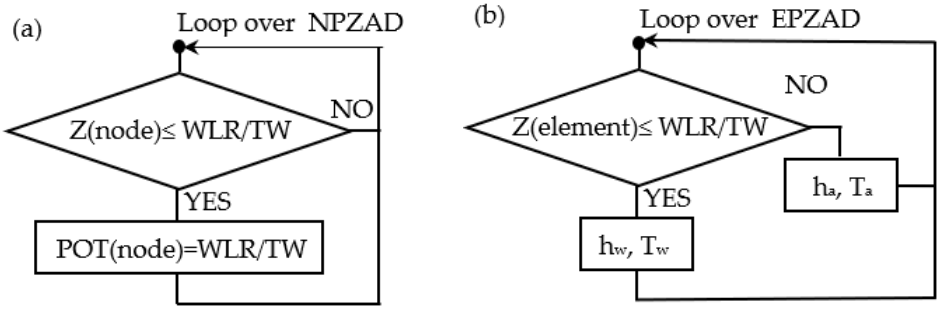

Figure 12. Flow chart of condition algorithm: (**a**) PAKV and (**b**) PAKT.

For the appropriate set of parameters and the given series of measured temperatures as contour conditions, a non-stationary thermal calculation was performed. A script was created, similar to the script shown in Figure 11, which runs PAKT. The temperature field inside the model was obtained by thermal calculation, based on which the values at the measuring points were calculated according to Equation (8). The resulting time series of temperature for each measuring point (thermometer in concrete) was printed in a separate file whose name was the symbol of the thermometer.

When calculating the temperature field in the concrete dam, another wrapper was created for the automatic prescription of boundary conditions analogous to the previously described calculation of underground water flow (seepage). An input file is also created for the calculation of the temperature field. On the elements (EPZAD) in the reservoir, "possible" heat transfer coefficients between water and concrete, as well as water and rock, are assigned. During the execution of the PAKT program, a check is performed if the z coordinate of the element center of gravity is lower than the water level in the reservoir (upstream) or tailwater (downstream), i.e., whether the element center of gravity is wetted. If the element is wetted, the heat transfer coefficient (h_w) between water and concrete or water and rock and water temperature (T_w) is set on the element surface. If the element center of gravity is dry, air to concrete or air to rock heat transfer coefficient (h_a) and air temperature (T_a) is prescribed on that element surface (Figure 12b).

The transient analysis was repeated with different sets of material parameters while calculating the sum of the squared deviations between measured and simulated temperature values. The calibration process was considered complete when the sum of squares was minimized for lamella 10. After calibration, the parameters were tested against other sets of boundary conditions to ensure their validity.

The calibration process was crucial for accurately predicting the dam's behavior under various weather conditions and ensuring stability.

5. Results and Discussions

A comparison of the measured and calculated values for the calibrated set of filtration parameters is presented. The numerically calculated potential values (Mp) at the measuring points are compared with the measured potential values and numerical values of the nearest neighbor node (Nn) (Figure 13). It can be seen that there is a difference between the numerical values at the measuring point and the numerical value of the nearest node. The difference depends on the distance between the measurement point and the nearest FE model node. This difference increases as the size of the element containing the measurement point increases. Using the interpolation algorithm presented in this paper, the average relative difference for pore pressure is reduced from 8.89% to 8.10% for the data shown in Figure 13.

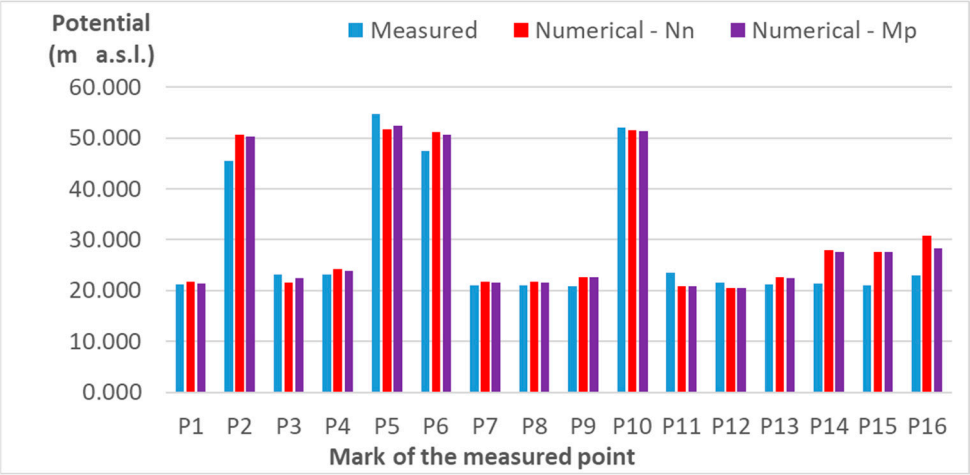

Figure 13. Measured potential vs. numerical potential values.

For the observed measuring points and adopted calibrated values, the individual relative deviation of the calculated piezometric level from the measured piezometric level was found to be 10.9% on average, with a standard deviation of 10.4%. Deviations between the measured and calculated values may result from the division of the surrounding terrain into quasi-homogeneous zones. The existing approach applied to the FEM model for defining these zones has shown some shortcomings, such as lack of continuity in the spatial distribution of some material zones. These problems highlighted the need for updates to the current FEM model, particularly in terms of the arrangement and continuity of quasi-homogeneous zones in the field.

The thermal finite element model of the dam was calibrated using available data obtained from thermometers. Transient thermal analysis for determining thermal distribution within the dam body at corresponding times and for corresponding reservoir water level and ambient temperature was performed. The measured temperatures and numerically calculated values at the measuring points in lamella ten are shown in Figures 14 and 15. The position of thermometers T60, T84, T87, and T90 is shown in Figure 4a. As can be seen for these figures, the measuring points T60 and T84 have better matching then measuring points T87 and T90.

The proposed algorithm was used for calibrating the filtration coefficients and thermal characteristics of concrete. The input parameters (boundary condition) for calibration were the measured values of the upper and lower water levels, air temperature, water temperature, and temperatures in the galleries. Calibration was carried out by comparing the measured values in piezometers/thermometers (in the work, measuring points) with the calculated values for selected boundary conditions (e.g., the elevation of the upper and lower water levels for the filtration calculation). The differences between the actual and measured values for the calibrated parameters are shown in Figures 13–15.

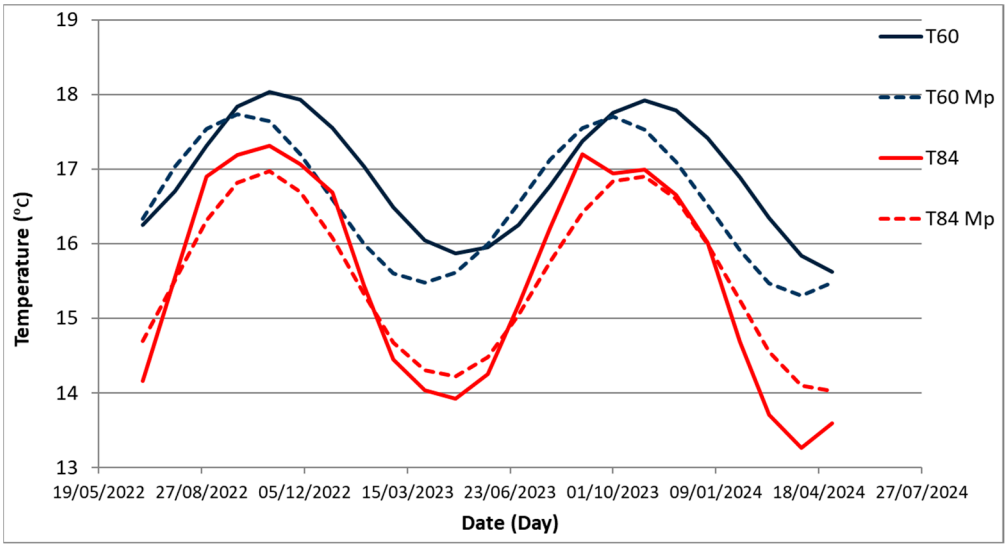

Figure 14. Measured temperature vs. numerical values at the measured point T60 and T84.

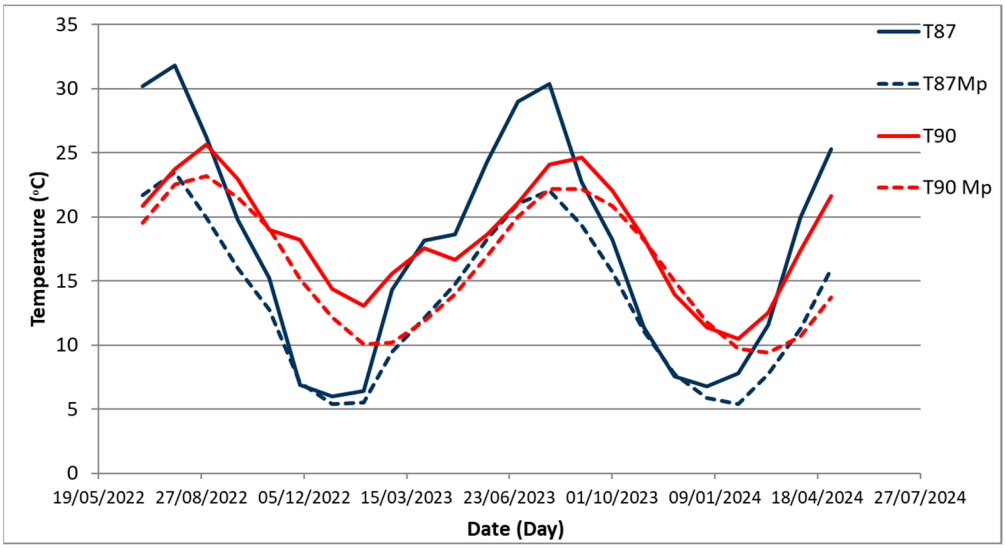

Figure 15. Measured temperature vs. numerical values at the measured point T87 and T90.

Pore pressure is a more appropriate numerical result for easy and accurate comparison. Pore pressure is only dependent on the Danube River level, while temperature is also affected by measured water and air temperatures, as well as wind conditions, sunlight, clouds, and rain, all of which have a significant impact on the difference between measured and predicted values. Figures 14 and 15 show that numerical simulation can predict temperature trends, but the variations between measured and computed values are much bigger than for pore pressure values. These variations could conceal the improvements made possible by interpolation, which are clearly seen in Figure 13, which displays pore pressure values.

The developed algorithm for determining the local coordinates of the measurement points was also used to map the calculated values from the 3D model to the 2D cross section. Two-dimensional cross sections are defined for display in the DMS web application. The cross sections are defined by the x coordinate (cross section normal to the river course) or y coordinate (cross section parallel to the river course).

First, a 2D cross section surface is created in the CAD 3D model of the dam. Then, a mesh of triangular linear finite elements is created on the cross section. The modified algorithm shown in Figure 6 is used to determine the element and local coordinates of

the nodes of the 2D cross section in the 3D model. The modifications of the algorithm in Figure 6 areas follows: input parameters are 3D elements and nodes of 2D cross section; output is an ASCI file that contains the ID of the 2D node, the ID of the 3D element in which the node is located, the coordinates of the 2D element, and the local coordinates. Equation (8) is used to calculate the potential/temperature values in the nodes of the 2D cross section. Figure 16 shows the potential field through the axis of lamella 10. The potential field in the 2D cross section is shown in Figure 16a, and the potential field through the 3D model is shown in Figure 16b.

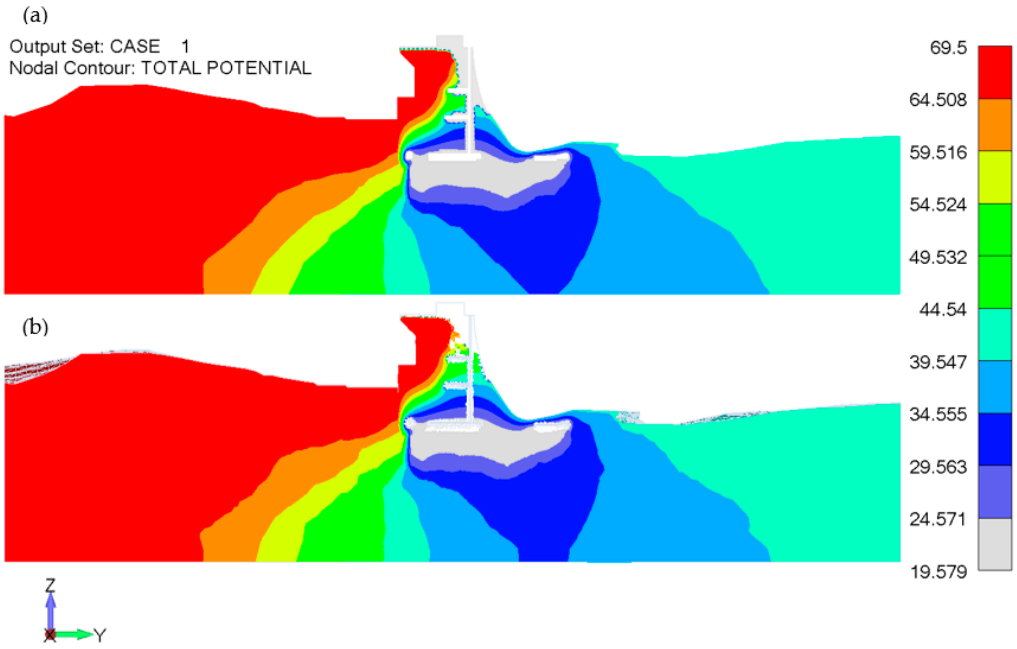

Figure 16. Potential field: (**a**) 2D cross section; (**b**) cut section in 3D model.

6. Conclusions

In this work, we presented a procedure for determining numerical values at the location of a measuring point when the actual position of the measuring point does not coincide exactly with one of the nodes of the finite element mesh. The proposed procedure is simple, efficient, and straightforward to implement:

- The initial step is the determination of the element in which the measuring point is located and calculating the local coordinates of the measuring point within the element.
- Numerical values at the measuring points are then calculated through interpolation using the local coordinates and numerical values at the nodes of the element.

The main motivation behind this work is to increase the robustness and adaptability of the Dam Monitoring System featuring the Finite Element Method software. This procedure can be utilized when additional instrument locations are added to the monitored system at a later time, allowing for the avoidance of remeshing of the numerical model. This procedure is applied to a dam structure, where potential and temperature are monitored through piezometers and thermometers, but it may be also be applied for other geomechanics problems, as well as engineering models in general. This algorithm can be particularly useful for academic, open source, and FEM solvers with narrow specialization, which lack the funding and development resources of commercial FEM solvers.

The results demonstrated that, following calibration, the numerically calculated values of potential/temperature with the new interpolation algorithm better matched the measured values, not significantly, but nevertheless, with noticeable improvement, which varies from measuring point to measuring point, with the average relative difference for pore pressure reduced from 8.89% to 8.10%. The procedure also reveals that the calibra-

tion procedure leads to the estimation of correct material properties which give accurate predictions of the potential and temperature validated by measured values.

Overall, the proposed procedure is simple yet effective. The modified finite element solvers, which can be altered by users and integrated into other software, greatly improve dam safety monitoring systems through enhanced data analysis and prediction capabilities, based on well-calibrated material properties and detailed, realistic finite element geometry. While commercial solvers can serve as a point of comparison and model validation, they cannot be modified by users or integrated into other software such are Dam Monitoring Systems.

Author Contributions: Conceptualization, S.V. and M.Z.; methodology, S.V.; software, S.V.; validation, S.V., M.T. and V.M.; formal analysis, M.T. and D.D.; investigation, S.V. and V.M.; resources, S.V.; data curation, D.D.; writing—original draft preparation, S.V.; writing—review and editing, S.V. and M.T.; visualization, S.V. and V.M.; supervision, M.Z.; project administration, M.Z.; funding acquisition, D.D. All authors have read and agreed to the published version of the manuscript.

Funding: This research was supported by the Science Fund of the Republic of Serbia, #GRANT No 7475, Prediction of damage evolution in engineering structures—PROMINENT; by the Ministry of Science, Technological Development and Innovation of the Republic of Serbia, contract No. 451-03-66/2024-03/200378; and by the Jaroslav Černi Water Institute, Belgrade, Serbia, contract No. 32/22/30-03/07, Development of integral FEM model of HPP "Djerdap 1" dam.

Data Availability Statement: The original contributions presented in the study are included in the article material; further inquiries can be directed to the corresponding author.

Conflicts of Interest: The authors declare no conflicts of interest.

References

1. Boretti, A.; Rosa, L. Reassessing the projections of the World Water Development Report. *npj Clean Water* **2019**, *2*, 15. [CrossRef]
2. Althoff, D.; Rodrigues, L.N.; da Silva, D.D. Evaluating Evaporation Methods for Estimating Small Reservoir Water Surface Evaporation in the Brazilian Savannah. *Water* **2019**, *11*, 1942. [CrossRef]
3. Tajziehchi, S.; Karbassi, A.; Nabi, G.; Yoo, C.; Ifaei, P. A Cost-Benefit Analysis of Bakhtiari Hydropower Dam Considering the Nexus between Energy and Water. *Energies* **2022**, *15*, 871. [CrossRef]
4. Adamo, N.; Al-Ansari, N.; Sissakian, V.; Laue, J.; Knutsson, S. Dams Safety: Inspections, Safety Reviews, and Legislations. *J. Earth Sci. Geotech. Eng.* **2020**, *11*, 109–143. [CrossRef] [PubMed]
5. Yang, L.; Liu, M.; Smith, J.A.; Tian, F. Typhoon Nina and the August 1975 Flood over Central China. *J. Hydrometeorol.* **2017**, *18*, 451–472. [CrossRef]
6. Kondolf, M.; Yi, J. Dam Renovation to Prolong Reservoir Life and Mitigate Dam Impacts. *Water* **2022**, *14*, 1464. [CrossRef]
7. Chen, X.; Hossain, F. Understanding Future Safety of Dams in a Changing Climate. *Bull. Am. Meteorol. Soc.* **2019**, *100*, 1395–1404. [CrossRef]
8. Valliappan, S.; Chee, C. Ageing Degradation of Concrete Dams Based on Damage Mechanics Concepts. In Proceedings of the International Symposium on Computational Structural Engineering, Shanghai, China, 22–24 June 2009.
9. Guo, X.; Dias, D.; Pan, Q. Probabilistic stability analysis of an embankment dam considering soil spatial variability. *Comput. Geotech.* **2019**, *113*, 103093. [CrossRef]
10. Siacara, A.T.; Napa-García, G.F.; Beck, A.T.; Futai, M.M. Reliability analysis of an earth dam in operating conditions. *SN Appl. Sci.* **2022**, *4*, 99. [CrossRef]
11. Omar-Darío, C.; Bernal, G.; Escovar, M.A. Flood and Drought Risk Assessment, Climate Change, and Resilience. In *Disaster Risk Reduction for Resilience Climate Change and Disaster Risk Adaptation*; Springer International Publishing: Berlin/Heidelberg, Germany, 2023; pp. 191–214.
12. Task Committee to Revise Guidelines for Dam Instrumentation. *Monitoring Dam Performance: Instrumentation and Measurements (ASCE Manual and Reports on Engineering Practice)*; CAB International: Wallingford, UK, 2018; p. 442.
13. Zhang, L.; Peng, M.; Chang, D.; Xu, Y. *Dam Failure Mechanisms and Risk Assessment*; John Wiley & Sons: Singapore, 2016; p. 450.
14. Li, B.; Yang, J.; Hu, D. Dam monitoring data analysis methods: A literature review. *Struct. Control Health Monit.* **2019**, *27*, e2501. [CrossRef]
15. Adamo, N.; Al-Ansari, N.; Sissakian, V.; Laue, J.; Knutsson, S. Dam Safety: Use of Seismic Monitoring Instrumentation in Dams. *J. Earth Sci. Geotech. Eng.* **2020**, *11*, 203–247. [CrossRef] [PubMed]
16. Ma, C.; Xu, X.; Yang, J.; Cheng, L. Safety Monitoring and Management of Reservoir and Dams. *Water* **2023**, *15*, 1078. [CrossRef]
17. Saeed, R.; Moradloo, A.J. A surrogate model for predicting dam displacement under seismic load for different orthotropic states of concrete. *Innov. Infrastruct. Solut.* **2024**, *9*, 115. [CrossRef]

18. Ramsheh, F.A.; Amini, M. FEM Simulation of Earth Dam and Comparison of Results with Field Monitoring (Case Study: Doroodzan Dam). *Spec. J. Min. Geol. Eng.* **2019**, *1*, 1–10.
19. Belmokre, A.; Mihoubi, M.K.; Santillán, D. Analysis of dam behavior by statistical models: Application of the Random Forest Approach. *KSCE J. Civ. Eng.* **2019**, *23*, 4800–4811. [CrossRef]
20. He, Q.; Gu, C.; Valente, S.; Zhao, E.; Liu, X.; Yuan, D. Multi-arch dam safety evaluation based on statistical analysis and numerical simulation. *Sci. Rep.* **2022**, *12*, 8913. [CrossRef]
21. Yu, Y.; Liu, X.; Wang, E.; Fang, K.; Huang, L. Dam safety evaluation based on multiple linear regression and numerical simulation. *Rock Mech. Rock Eng.* **2018**, *51*, 2451–2467. [CrossRef]
22. Prakash, G.; Dugalam, R.; Barbosh, M.; Sadhu, A. Recent advancement of concrete dam health monitoring technology: A systematic literature review. In *Structures*; Elsevier: Amsterdam, The Netherlands, 2022.
23. Xiu, D.H.; Zhou, Q.Z.; Li, Y.; Wu, L.X. Dam Safety Analysis Based on Stepwise Regression Model. *Adv. Mater. Res.* **2011**, *204*, 2158–2161.
24. Grujovic, N.; Divac, D.; Zivkovic, M.; Slavkovic, R.; Milivojevic, N.; Milivojevic, V.; Rakic, D. An inelastic stress integration algorithm for a rock mass. *Acta Geotechica* **2013**, *8*, 265–278. [CrossRef]
25. Hariri-Ardebili, A.M.; Mirzabozorg, H.G.M.; Akhavan, A.; Amini, R. Calibration of 3D FE model of DEZ high arch dam in thermal and static conditions using instruments and site observation. In Proceedings of the 6th International Conference on Dam Engineering, Lisbon, Portugal, 15–17 February 2011.
26. Mirzabozorg, H.; Hariri-Ardebili, M.; Heshmati, M.; Seyed-Kolbadi, S. Structural safety evaluation of Karun III Dam and calibration of its finite element model using instrumentation and site observation. *Case Stud. Struct. Eng.* **2014**, *1*, 6–12. [CrossRef]
27. Wang, Z.; Liu, S.; Vallejo, L.; Wang, L. Numerical analysis of the causes of face slab cracks in Gongboxia rockfill dam. *Eng. Geol.* **2014**, *181*, 224–232. [CrossRef]
28. Divac, D.; Vuckovic, D.; Zivkovic, M.; Vulovic, S. Reservoir, dam and rock mass interaction modeling. In Proceedings of the Sixth European Conference on Numerical, Graz, Austria, 6–8 September 2006.
29. Dwivedi, D.; Saraf, A.; Das, J. Geoinformatics-based investigation of slope failure and landslide damming of Chenab River, Lahaul-Spiti, Himachal Pradesh, India. *Nat. Hazards Res.* **2023**, *3*, 186–195. [CrossRef]
30. Shirazi, M.G.; Rashid, A.S.B.A.; Ganiyu, A.A. Analysis of seepage control system improvement in an earthen dam. *Dams Reserv.* **2022**, *33*, 27–33. [CrossRef]
31. Naeini, M.; Akhtarpour, A. Numerical analysis of seismic stability of a high centerline tailings dam. *Soil Dyn. Earthq. Eng.* **2018**, *107*, 179–194. [CrossRef]
32. Hemeda, S. Geotechnical modelling and subsurface analysis of complex. *Int. J. Geo-Eng.* **2022**, *13*, 9. [CrossRef]
33. Ledesma, O.; Sfriso, A.; Manzanal, D. Procedure for assessing the liquefaction vulnerability of tailings dams. *Comput. Geotech.* **2022**, *144*, 104632. [CrossRef]
34. Ya, S.; Eisenträger, S.; Qu, Y.; Zhang, J.; Kuen, T.; Song, C. Seismic analysis of post-tensioned concrete gravity dams using scaled boundary finite elements implemented as ABAQUS UEL. *Soil Dyn. Earthq. Eng.* **2023**, *164*, 107620. [CrossRef]
35. Patra, K.B.; Segura, R.L.; Bagchi, A. Modeling Variability in Seismic Analysis of Concrete Gravity Dams: A Parametric Analysis of Koyna and Pine Flat Dams. *Infrastructures* **2024**, *9*, 10. [CrossRef]
36. Zhong, X.; Sun, X.N.; Tang, K.D. Static and Dynamic Analysis of Concrete Gravity Dam by ANSYS. *Appl. Mech. Mater.* **2013**, *438*, 1334–1337. [CrossRef]
37. Xunqiang, Y.; Jianbo, L.; Chenglin, W.; Gao, L. ANSYS implementation of damping solvent stepwise extraction method for nonlinear seismic analysis of large 3-D structures. *Soil Dyn. Earthq. Eng.* **2013**, *44*, 139–152. [CrossRef]
38. Oliveira, S.; Alegre, A.; Carvalho, E.; Mendes, P.; Proença, J. Seismic and structural health monitoring systems for large dams: Theoretical, computational and practical innovations. *Bull. Earthq. Eng.* **2022**, *20*, 4483–4512. [CrossRef]
39. EPS Homepage. Elektroprivreda Srbije (EPS). Available online: https://www.eps.rs/eng/Poslovanje-EE/Pages/Hidroelektrane.aspx (accessed on 22 August 2024).
40. Hidrotehnika Homepage. Hidrotehnika. Available online: https://hidrotehnika.rs/brane/srbija/derdap/ (accessed on 22 August 2024).
41. Zheng, P.; Yang, Y.; Liu, Z.; Xu, Q.; Wang, J.; Leng, J.; Liu, T.; Zhu, Z.C.J. Parallel and automatic isotropic tetrahedral mesh generation of misaligned assemblies. *CCF Trans. High Perform. Comput.* **2020**, *2*, 149–163. [CrossRef]
42. Bathe, K.-J. *Finite Element Procedures*; Prentice Hall: Upper Saddle River, NJ, USA, 2007.
43. Siemens. *Femap User Guide Version 11.2*; Siemens PLM Software Inc.: Plano, TX, USA, 2015.
44. Vulović, S.; Bojović, M.; Topalović, M. Automation of FEM Analysis Report Generation using Visual Basic FEMAP API. In Proceedings of the 10th International Conference on Information Society and Technology ICIST 2020, Kopaonik, Serbia, 8–11 March 2020.
45. Siemens. *Femap API Reference*; Siemens Digital Industries Software Inc.: Plano, TX, USA, 2015.
46. Meng, M.; Steinhardt, S.; Schubert, A. Application Programming Interface Documentation: What Do Software Developers Want? *J. Tech. Writ. Commun.* **2018**, *48*, 295–330. [CrossRef]
47. Vulović, S.; Pavlović, D.; Živković, M.; Vujanac, R.; Topalović, M. Analysis of freight wagons for transporting of bulk materials. In Proceedings of the 5th Serbian-Greek Symposium on Advanced Mechanics, Kragujevac, Serbia, 28–30 June 2021.

48. Rakić, D.; Stojković, M.; Ivetić, D.; Živković, M.; Milivojević, N. Failure Assessment of Embankment Dam Elements: Case Study of the Pirot Reservoir System. *Appl. Sci.* **2022**, *12*, 558. [CrossRef]
49. Grujović, N.; Dunić, V.; Divac, D.; Vulović, S. Hydropower dam thermal numerical model calibration methodology. In Proceedings of the 7th International Conference, Kopaonik, Serbia, 12–15 March 2017.
50. Stojanovic, B.; Milivojevic, M.; Ivanovic, M.; Milivojevic, N.; Divac, D. Adaptive system for dam behavior modeling based on linear regression and genetic algorithms. *Adv. Eng. Softw.* **2013**, *65*, 182–190. [CrossRef]
51. Stojanovic, B.; Milivojevic, M.; Milivojevic, N.; Antonijevic, D. A self-tuning system for dam behavior modeling based on evolving artificial neural networks. *Adv. Eng. Softw.* **2016**, *97*, 85–95. [CrossRef]
52. Topalović, M.; Vulović, S.; Živković, M.; Bojović, M. Combination of Bash and Python in Development of Wrappers used for Automation of Finite Element Analysis. In Proceedings of the 10th International Conference on Information Society and Technology ICIST 2020, Kopaonik, Serbia, 8–11 March 2020.